Volume 1 | Number 1 | Jan 2013 | Pages 1–100

Journal of
Materials Chemistry A

Materials for energy and sustainability
www.rsc.org/materialsA

Li⁺

e⁻

Li⁺

e⁻

Li⁺

Li⁺

ROYAL SOCIETY
OF CHEMISTRY

ROYAL SOCIETY
OF CHEMISTRY

www.rsc.org/materialsA

Metal organic frameworks-derived Co_3O_4 hollow dodecahedrons with controllable

interiors as outstanding anodes for Li storage

Jie Shao,[‡ a,c] Zhongming Wan,[‡ a] Hongmei Liu,[a] Huiyuan Zheng,[a] Tian Gao,[a] Ming

Shen,[b] Qunting Qu,*[,a] and Honghe Zheng *[,a]

[a] *School of Energy & Collaborative Innovation Center of Suzhou Nano Science and Technology, Soochow University, Suzhou Jiangsu 215006, China.*
[b] *Huasheng Chemical Corporation, Zhangjiagang, Jiangsu 215635, China*
[c] *College of Chemistry, Chemical Engineering and Material Science, Soochow University, Suzhou Jiangsu 215006, China*
E-mail: qtqu@suda.edu.cn; hhzheng@suda.edu.cn
‡ Equal contribution.

Abstract

Hollow Co_3O_4 dodecahedrons with controllable interiors are prepared through direct

pyrolysis of Co-based zeolitic imidazolate framework (ZIF-67) rhombic

dodecahedrons. The ball-in-dodecahedron Co_3O_4 manifests an extremely high

reversible capacity of 1550 mAh g^{-1} and excellent cycling stability (1335 mAh g^{-1}

after 100 cycles), rendering it a promising candidate for practical application in next

generation of high-energy Li-ion batteries.

Introduction

The ever-increasing shortage of fossil fuels in the whole world is accelerating the development of energy storage and conversion systems. Currently, lithium-ion batteries (LIBs) are the predominant power sources for portable electronic devices because of their high energy, long lifespan, no memory effect, and environmental benignity. They are also showing great prospect in large-scale applications of electric vehicles and hybrid electric vehicles.[1-2] Co_3O_4, as a promising candidate material for anode of LIBs, has been paid more and more attentions due to its much higher theoretical capacity of 890 mAh g^{-1} than that of conventional graphite (372 mAh g^{-1}).[3-13] Nonetheless, similar to other metal oxide anodes that store Li through conversion reactions, Co_3O_4 undergoes significant volume expansion/contraction during lithiation/delithiation cycles. The ensuing large strains cause pulverization of electrode materials and loss of electronic contact, thereby resulting in rapid capacity decay. In order to circumvent these obstacles, one of the most effective protocols is to fabricate hollow materials (especially those with complex interiors) constructed by nanometer-scaled building blocks.[3, 9, 14] These unique structures can not only shorten the diffusion distance of Li^+ and increase the electrode-electrolyte contact area, but also provide additional voids to buffer the volume changes. Dan Wang et al.[5] presented the accurate control of multi-shelled Co_3O_4 microspheres using pre-formed carbon microspheres as sacrificial templates. The as-prepared triple-shelled Co_3O_4 microspheres exhibit an outstanding discharge capacity of 1616 mAh g^{-1} at the 30th cycles, which is the highest capacity value among all the Co_3O_4-based materials

reported so far. Albeit with such good performance for Li storage, the templating synthetic method involves tedious multistep procedures. Preparation of hollow Co_3O_4 materials with complex interiors through a simpler and more scalable method remains a great challenge.

Metal-organic frameworks (MOFs), formed by supramolecular assembly of metal ions (or metal clusters) with electron-donating organic ligands, possess the advantages of high surface areas, adjustable pore sizes, and controllable architectures.[15-16] Most importantly, by taking advantage of their thermal behavior and chemical reactivity, various porous carbons and metal oxides can be achieved easily through direct pyrolysis of MOFs.[17-21] For instance, microporous carbon polyhedrons were produced through calcination of Zn-based MOFs (ZIF-8) under inert atmosphere.[22] Pyrolysis of a typical Fe-based MOF (MIL-88-Fe) generated spindle-like mesoporous Fe_2O_3 comprising of clustered Fe_2O_3 nanoparticles.[18] David Lou et al.[20] succeeded in the scalable synthesis of hollow Fe_2O_3 microboxes through simultaneous oxidative decomposition of Prussian blue microcubes and crystal growth of iron oxide shells. Spherical multi-ball-in-ball hybrid metal oxides were prepared utilizing the corresponding MOFs as precursors.[23] Novel CuO/Cu_2O hollow polyhedrons were fabricated through thermal decomposition of $[Cu_3(btc)_2]_n$ (btc=benzene-1,3,5-tricarboxylate) polyhedrons.[24] Nonetheless, a controllable synthesis of hollow Co_3O_4 with complex interiors for LIBs application through direct pyrolysis of Co-based MOFs has not been reported yet.[25]

In this work, we present a facile and scalable method to synthesize Co_3O_4 hollow dodecahedrons with complex interiors. A Co-based zeolitic imidazolate framework, ZIF-67, is synthesized through a solution-precipitation method and used as precursor. Two different types of hollow Co_3O_4 structures with uniform dodecahedral morphologies (ball-in-dodecahedron and concave-dodecahedron) can be obtained by tuning the pyrolysis procedures of ZIF-67. For application as anode material of LIBs, the ball-in-dodecahedron Co_3O_4 manifests an extremely high reversible capacity of 1550 mAh g^{-1} and excellent cycling stability (1335 mAh g^{-1} after 100 cycles).

Results and discussion

ZIF-67 is one of the most well-known and easily-available Co-based MOFs, so we employ it as the precursor to synthesize Co_3O_4. Monodisperse ZIF-67 rhombic dodecahedrons were fabricated by mixing cobalt salts (cobalt nitrate or acetate) and 2-methylimidazole in methanol solvent. Precipitation of ZIF-67 took place when the mixture solutions were left unstirred and aged at ambient temperature for 24 h. It is noteworthy that the particle sizes of ZIF-67 crystals were well controlled from nanometer scale to micrometer scale by adjusting the reaction conditions (see ESI†). Scanning electron microscope (SEM) images of three types of ZIF-67 rhombic dodecahedrons are shown in **Fig. 1**. Their average particle sizes are determined to be 100 nm, 800 nm, and 2 μm, respectively. The different nucleation rate of ZIF-67 associated with the coordination reaction between Co^{2+} ions and 2-methylimidazole is believed to be responsible for the varying particle sizes.[16, 26] For the middle-sized ZIF-67, cobalt nitrate and 2-methylimidazole were first dissolved in methanol

separately to form two solutions, and then a mixture solution was obtained by slowly adding 2-methylimidazole solution into cobalt nitrate solution. When two dry powders of cobalt nitrate and 2-methylimidazole were first mixed together, followed by addition of methanol, a faster nucleation of ZIF-67 occurred owing to the instantaneous high concentration of both Co^{2+} ions and 2-methylimidazole. Consequently, a large number of minute nuclei were formed, which shortened the crystal growth stage and resulted in small-sized particles. When cobalt nitrate was replaced with cobalt acetate, the strong interaction between Co^{2+} and CH_3COO^- slowed down the coordination reaction of Co^{2+} ions with 2-methylimidazole. The slow nucleation rate gave rise to a smaller amount of ZIF-67 nuclei, and elongated the crystal growth stage. As a result, large-sized particles were obtained. The inset in Fig. 1e shows the simulated dodecahedral structure of ZIF-67, in which all the faces are rhombic, and the vertex share three or four edges. SEM images of as-prepared ZIF-67 clearly disclose the typical two kinds of vertex in dodecahedron that share three or four edges.

We first take the middle-sized ZIF-67 dodecahedrons for example to probe the feasibility of utilizing ZIF-67 as precursor to prepare Co_3O_4 material. **Fig. 2**a presents the X-ray diffraction (XRD) pattern of ZIF-67. All the diffraction peaks match well with the simulated patterns published in literatures.[27] N_2 adsorption/desorption isotherm of ZIF-67 (Fig. 2b) exhibits a type-I isotherm with a sharply increased adsorption at low relative pressure, which is characteristic of microporous material. The specific surface area of ZIF-67 calculated through Brunauer-Emmett-Teller (BET)

method is 1262 m^2 g^{-1}, suggesting its highly developed porous structure. Thermal behavior of ZIF-67 was investigated through thermogravimetric (TG) analysis (Fig. 2c), which indicated that ZIF-67 underwent a drastic weight loss between 340 °C and 405 °C and remained 36% of its original weight when subjected to heat treatment under air atmosphere. As the temperature continued to rise, no weight loss was observed, signifying the complete decomposition of organic ligands of ZIF-67 and simultaneous formation of Co_3O_4 at temperature above 340 °C. Therefore, we first adopted a one-step calcination process to pyrolyze ZIF-67 under the flow of air. The temperature was raised from room temperature to 350 °C at a ramping rate of 1 °C/min, and then stabilized at 350 °C for 2h.

XRD pattern of the product after one-step calcination of ZIF-67 (Fig. 2d) confirms that pure Co_3O_4 spinel phase with a face-centered cubic lattice (JCPDF Card No. 42-1467, cell parameter a=8.084 Å) is obtained. The average crystallite size of Co_3O_4 calculated from XRD data using Scherrer equation is estimated to be 18 nm. In addition, the obtained Co_3O_4 material exhibits no weight loss upon TG analysis (Fig. S1†), excluding the possibility that some undecomposed organic ligands may be left in the ultimate material.

SEM images (**Fig. 3**a-c) of Co_3O_4 reveal that the polyhedral morphology of ZIF-67 is preserved perfectly after one-step calcination. Uniform dodecahedrons are observed, and the typical two kinds of vertex that share four or three edges also can be seen obviously. In sharp contrast with the smooth surface of ZIF-67, the surface of Co_3O_4 dodecahedrons is composed of numerous primary particles and interstices. From the

cracked parts of one broken Co_3O_4 dodecahedron (Fig. 3c), we can see that the interior contains a spherical core as well as a large void between the shell and core. So this material is described as ball-in-dodecahedron Co_3O_4. TEM image of Co_3O_4 (Fig. 3d) further confirms that this material possesses the ball-in-polyhedron structure, as manifested by the black round cores and grey areas sandwiched between the cores and polyhedral edges. In addition, the inner cores are not purely solid and contain many pores inside as indicated by the arrows. The particle size of primary building blocks of ball-in-dodecahedron Co_3O_4 is visually determined to be about 18 nm (see TEM image at high magnification in Fig. S2†), in good accordance with the value estimated from XRD pattern. N_2 adsorption/desorption isotherms were measured to study the porous structure of ball-in-dodecahedron Co_3O_4 (Fig. S3†). The BET surface area is determined to be 45 m^2 g^{-1}. The corresponding pore-size distribution curve presents a broad peak centered at about 25 nm, indicating the mesoporous structure of the obtained Co_3O_4. It can be concluded from the above results that a hollow Co_3O_4 with ball-in-dodecahedron structure can be achieved easily through direct pyrolysis of ZIF-67. Actually, preparation of hollow particles from MOFs always needs the assistance of sacrificial hard templates or involves multi-step procedures, which are complex and time-consuming.[16, 28] Thus, the method for the fabrication of hollow Co_3O_4 herein through direct pyrolysis of ZIF-67 is simpler and more scalable.

The formation mechanism of such a ball-in-dodecahedron Co_3O_4 through calcination of ZIF-67 dodecahedrons is considered to be similar to that of yolk-shell microspheres derived from thermal decomposition of solid precursors.[29] A

heterogeneous contraction process caused by non-equilibrium heat treatment is utilized to illustrate this phenomenon.[30] A schematic is shown in **Fig. 3e** to illustrate the formation of this ball-in-dodecahedron hollow structure. At the initial stage of calcination, there exists a large temperature gradient (ΔT) along the radical direction of ZIF-67 dodecahedrons. As a result, a Co_3O_4 dodecahedral shell is first formed on the surface of ZIF-67 core. As the calcination continues, two forces with opposite directions are supposed to act on the interface between the Co_3O_4 shell and ZIF-67 core due to the gradual decomposition of ZIF-67. The contraction force (Fc) associated with the formation of Co_3O_4 crystallites leads to the inward contraction of Co_3O_4 core, meanwhile, the adhesive force (Fa) resulting from the release of gases prevents the inward contraction of Co_3O_4 outer shell. At last, the Co_3O_4 core and shell are separated by large voids. To the best of our knowledge, Co_3O_4 has never been fabricated into such a unique ball-in-dodecahedron structure.

Considering that variation of calcination atmosphere may greatly influence the morphology of the ultimate product,[18] another two-step calcination route was implemented in this study. Specifically, ZIF-67 was first pyrolyzed at 500 °C under the protection of N_2 gas and then annealed at 350 °C in flowing air. To our delight, a new Co_3O_4 material with totally different morphology was obtained. SEM images of Co_3O_4 (**Fig. 4**a and b) show that this material possesses a homogeneous dodecahedral morphology but with concave surfaces. So this material is denoted as concave-dodecahedron Co_3O_4. We assume that, the organic ligands of ZIF-67 probably crosslinked together during the first-step heat treatment in N_2, which make

the surfaces of dodecahedrons curve inward. In order to verify this assumption, TG

behavior of ZIF-67 under N_2 atmosphere was first investigated. As shown in Fig. 2c,

ZIF-67 starts to lose weight at a much higher temperature of about 500 $^{\circ}$C and

maintained a higher weight percentage of 56% as compared with those observed in air

(340 $^{\circ}$C and 36%, respectively). These results suggest that the organic ligands of

ZIF-67 should crosslink together instead of decompose directly after calcination at

500 °C under the protection of N_2. In addition, SEM images, TG behavior, and X-ray

photoelectron spectra (XPS) of the intermediate product (after the first-step

calcination of ZIF-67) were analyzed. The concave surfaces of the intermediate

product (Fig. 4c) suggest that shrinkage of dodecahedral precursor occurred during

the first-step heat treatment. The drastic weight loss of about 38% for the intermediate

products upon TG analysis (Fig. S4†) as compared with the negligible weigh loss of

Co_3O_4 obtained through one-step calcination of ZIF-67 in air also signifies that, the

five-membered rings of 2-methylimidazole in ZIF-67 underwent crosslinking reaction

rather than oxidative decomposition during the first-step calcination at 500 °C under

N_2 atmosphere. XPS results (Fig. S5†) suggest that the crosslinking product of these

organic ligands is probably amorphous carbon. By comparing the SEM images of

Co_3O_4 and intermediate product, it can be seen that the structure of intermediate

product is more flexible as compared with the rigid edges of Co_3O_4, suggesting that

the first-step calcination of ZIF-67 probably results in formation of carbon-supported

materials. Therefore, it can be concluded that the crosslinking reaction of organic

ligands leads to the contraction of dodecahedron.

TEM images of concave-dodecahedron Co_3O_4 taken from different perspectives are shown in Fig. 4d and S6†. As manifested by the sharp contrast between grey centers and black edges, this structure can be considered as hollow dodecahedrons. Also, these Co_3O_4 dodecahedrons are composed of primary nanoparticles with dimension of about 24 nm, slightly larger than the former ball-in-dodecahedron Co_3O_4. Formation of such a pure hollow structure without filled cores is schematically illustrated in Fig. 4e. During the first-step calcination, the crosslinking products of the organic ligands of ZIF-67 (amorphous carbon) serve as a temporary framework to distribute Co or CoO_x particles. Meanwhile, the surfaces of dodecahedrons contract inward. During the second-step calcination under air atmosphere, the outward force induced by the release of gases from oxidization of carbon lead to the outward diffusion of Co or CoO_x particles, which are simultaneously oxidized to Co_3O_4 by air. For comparison, the BET surface area of concave-dodecahedron Co_3O_4 is 16 $m^2 g^{-1}$ (Fig. S7†), smaller than that of ball-in-dodecahedron Co_3O_4. XRD pattern, TG curve, and Raman spectrum of the ultimate Co_3O_4 material (Fig. 2d, S8† and S9†) suggest that there are no residual carbons or organic chains in this material. As a result, hollow Co_3O_4 dodecahedrons with high purity are obtained through two-step calcination of ZIF-67.

The electrochemical performances of ball-in-dodecahedron and concave-dodecahedron Co_3O_4 for Li-ion storage were tested using Li foil as both counter and reference electrodes. The working voltage was set between 3.0 V and 0.01 V, a typical voltage range for the anode material of LIBs. The initial three discharge/charge curves of Co_3O_4 at the current density of 100 mA g^{-1} are shown in

Fig. 5a. The initial discharge capacities of ball-in-dodecahedron and concave-dodecahedron Co_3O_4 are 1735 and 1083 mAh g^{-1}, respectively, which can be ascribed to the conversion reaction of Co_3O_4 to Co and Li_2O, and formation of solid-electrolyte-interface (SEI) film.[5, 31-32] Remarkably, the reversible (charge) capacities of ball-in-dodecahedron Co_3O_4 during the first three cycles are 1118, 1168, and 1220 mAh g^{-1}, respectively, far exceeding the theoretical capacity of Co_3O_4. Since the coulombic efficiency after the first cycle is stabilized at about 96%, the extremely high capacity of ball-in-dodecahedron Co_3O_4 should relate to the reversible formation/decomposition of polymer/gel-like layer on the surface of Co_3O_4 active material[4] or an interfacial lithium-storage.[11, 33-34] Very recently, solid-state NMR technique was employed to study the conversion reaction of metal oxide (RuO_2), which reveals that the extra capacity of RuO_2 is mainly because of the generation of LiOH and its subsequent reversible reaction with Li to form Li_2O and LiH.[35] This mechanism may also be applicable to Co_3O_4. Obviously, the ball-in-dodecahedron Co_3O_4 exhibits a much higher capacity than the concave-dodecahedron Co_3O_4. The reasons can be mainly attributed to the following two aspects. On the one hand, the smaller size of primary nanoparticles in ball-in-dodecahedron Co_3O_4 and higher surface area of ball-in-dodecahedron Co_3O_4 can shorten the diffusion distance of Li$^+$ and increase the electrode/electrolyte contact areas, thereby enhancing the utilization efficiency of active materials. On the other hand, the unique structure of ball-in-dodecahedron Co_3O_4 with filled cores is superior to the pure hollow structure of concave-dodecahedron Co_3O_4. It is proposed that an appropriate volume-occupying

ratio of material can increase the fraction of electrochemically active component and guarantee a high volumetric specific capacity. Similar phenomenon was also observed for the Co_3O_4 hollow microspheres with complex interiors, where the capacity of triple-shelled Co_3O_4 was clearly superior to those of single- and double-shelled Co_3O_4.[5]

The capacity evolution of the two Co_3O_4 materials during long-term cycling at a current density of 100 mA g^{-1} is shown in Fig. 5b. Interestingly, the capacity of ball-in-dodecahedron Co_3O_4 increased gradually during the initial 20 cycles, and then after a slight decrease, the capacity began to rise once again. Such a two-round increase of capacity is considered to be associated with the two activation process of the electrodes taking the multilevel structure of ball-in-dodecahedron Co_3O_4 into account.[31] The first- and second-round increase of capacity may correspond to the activation process of outer shell and inner core, respectively. The polymer/gel-like layer that contributes to the high capacity of Co_3O_4 may build up slowly over a number of cycles.[4, 36] However, the ensuing capacity loss after each-round increase of capacity suggest that some components of polymer/gel-like layer may be unstable upon repetitive cycles. An extremely high reversible capacity of about 1550 mAh g^{-1} is reached after 60 cycles, which then declines slowly with 1335 and 1265 mAh g^{-1} of capacity retained after 100 and 140 cycles, respectively. Actually, the reversible capacity of Co_3O_4-based materials (including Co_3O_4/carbon composites) in most literatures lies between 700 and 1200 mAh g^{-1},[3-4, 6-9, 11, 14] and an outstanding high capacity of about 1500 mAh g^{-1} is also reported.[5] It is notable that the Li-storage

capability of ball-in-dodecahedron Co_3O_4 is prominent as compared with other Co_3O_4 materials reported previously.

In the case of concave-dodecahedron Co_3O_4, the capacity declines slowly during the initial 30 cycles, followed by a drastic capacity loss during the subsequent 15 cycles. After that, the capacity keeps at a constant value of about 640 mAh g^{-1} until 100 cycles. The distinct cycling behaviors of ball-in-dodecahedron and concave-dodecahedron Co_3O_4 further demonstrate the superiority of core-filled hollow structure. The filled cores, large voids[37] as well as small particle size of ball-in-dodecahedron Co_3O_4 can effectively stabilize the hollow polyhedral structure. In contrast, the hollow polyhedral structure of concave-dodecahedron Co_3O_4 may easily collapse into small particles during the repeated lithiation/delithiation cycles, which explains the sudden capacity loss between the 30th and 45th cycles.

Rate behavior of Co_3O_4 is another important metric that needs to be considered for application in LIBs. The reversible capacities of ball-in-dodecahedron and concave-dodecahedron Co_3O_4 cycled at various current rates are shown in Fig. 5c. With the current density increases, the capacity of the two materials decreases stepwise. Notably, even at the current density of 2000 mA g^{-1}, the ball-in-dodecahedron Co_3O_4 still delivers a capacity of 650 mAh g^{-1}, considerably higher than the capacities of Co_3O_4 nanomesh (380 mAh g^{-1} at 1000 mA g^{-1}),[10] graphene/Co_3O_4 (493 mAh g^{-1} at 1500 mA g^{-1})[31] and onion-like carbon/Co_3O_4 nanocomposites (154 mAh g^{-1} at 2000 mA g^{-1}).[6] When the current density returns to 100 mA g^{-1}, a high capacity of 1500 mAh g^{-1} still can be reached for the

ball-in-dodecahedron Co_3O_4. The above excellent high-rate capability of ball-in-dodecahedron Co_3O_4 can be attributed to its hollow porous structure and nanoscaled building blocks, which not only facilitate access of electrolyte but also shorten diffusion distances of lithium ions and electrons.

Conclusions

In conclusion, a simple and scalable method was presented to synthesize Co_3O_4 dodecahedrons with complex interiors through direct pyrolysis of Co-based MOFs (ZIF-67). Two different types of hollow structures, namely, ball-in-dodecahedron and concave-dodecahedron Co_3O_4, were obtained through one-step and two-step calcination of ZIF-67, respectively. The formation mechanisms of these unique hollow structures were also discussed. When being used as the anode material of LIBs, the ball-in-dodecahedron Co_3O_4 manifested an outstanding performance as compared with the concave-dodecahedron Co_3O_4 and other reported Co_3O_4 materials. The facile synthesis and excellent performance of ball-in-dodecahedron Co_3O_4 render it a promising candidate for practical application in next generation of high-energy LIBs.

Experimental details

Synthesis of ZIF-67 dodecahedrons: Monodisperse ZIF-67 rhombic dodecahedrons were fabricated by mixing cobalt salts and 2-methylimidazole in methanol solvent. For the synthesis of middle-sized ZIF-67, 4.0 mmol of cobalt nitrate hexahydrate and 8.0 mmol of 2-methylimidazole were first dissolved separately in 50 mL methanol, and then the latter clear solution was added slowly into the former pink solution upon stirring at room temperature. When the two solutions were mixed together stirring

was stopped. Precipitation of ZIF-67 took place when the mixture solution was left unstirred and aged for 24 h. At last, the purple precipitate was collected by centrifugation, washed with ethanol, and dried at room temperature. In the case of small-sized ZIF-67, two dry powders of cobalt nitrate (4.0 mmol) and 2-methylimidazole (8.0 mmol) were first mixed together, followed by addition of methanol (100 mL) under stirring with magnetic stirrer. When the two powders were dissolved completely stirring was stopped. The subsequent procedures were the same as those of middle-sized particles. Large-sized ZIF-67 was prepared through the similar method to that of middle-sized ZIF-67 except that cobalt nitrate hexahydrate was replaced with cobalt acetate tetrahydrate.

Synthesis of Co_3O_4 hollow dodecahedrons: Ball-in-polyhedron Co_3O_4 was prepared through one-step calcination of ZIF-67 in a tube-oven under the flow of air. The temperature was raised from room temperature to 350 °C at a ramping rate of 1 °C/min, and then stabilized at 350 °C for 2h. Concave-dodecahedron Co_3O_4 was prepared through a two-step calcination route. Specifically, ZIF-67 was first pyrolyzed at 500 °C under the protection of N_2 gas and then annealed at 350 °C in flowing air. The ramping rate was also set at 1 °C/min.

Characterization methods: XRD was collected using a Rigaku D/MAX-IIA X-ray diffractometer with Cu Kα radiation. TG analysis was carried out with a SEIKO TG/DTA 7300 thermal analyzer. FE-SEM images were obtained using Hitachi SU8000 equipment operated at 25 kV. TEM images were obtained using Philips EM 420 transmission electron microscope. XPS was operated on VG ESCA 2000

equipment. Raman spectrum was measured through JobinYvon LabRAM HR800

Raman spectrometer. N_2 adsorption/desorption isotherm and the BET surface area was

measured using Micromeritics TriStar II apparatus with liquid nitrogen at 77 K.

Electrochemical testing: The working electrode slurry was prepared by dispersing

Co_3O_4, Super P-Li and poly(vinylidene fluoride) (PVDF) binder in

N-methylpyrrolidone with a weight ratio of 8/1/1. The slurry was spread onto copper

foil disks and dried in a vacuum oven at 120 ^{o}C overnight. Lithium foil as the counter

and reference electrode, and 1.0 M $LiPF_6$ in ethyl carbonate/dimethyl carbonate (1:1

v/v ratio) as the electrolyte, Celgard 2500 as the separator, were used to assemble a

CR2032 coin cell. Galvanostatic discharge and charge tests were performed with a

cycle tester from LAND Electronic Co., and the cut-off potential window of Co_3O_4

was set between 3.0 V and 0.01 V.

Acknowledgements

Notes and references

[a] *School of Energy & Collaborative Innovation Center of Suzhou Nano Science and Technology, Soochow University, Suzhou Jiangsu 215006, China.*
[b] *Huasheng Chemical Corporation, Zhangjiagang, Jiangsu 215635, China*
[c] *College of Chemistry, Chemical Engineering and Material Science, Soochow University, Suzhou Jiangsu 215006, China*
E-mail: qtqu@suda.edu.cn; hhzheng@suda.edu.cn

1   M. Armand and J. M. Tarascon, *Nature*, 2008, **451**, 652-657.

2   B. Kang and G. Ceder, *Nature*, 2009, **458**, 190-193.

3   D. Liu, X. Wang, X. Wang, W. Tian, Y. Bando and D. Golberg, *Sci. Rep.*, 2013, **3**, 2543.

4   J. Zhu, L. Bai, Y. Sun, X. Zhang, Q. Li, B. Cao, W. Yan and Y. Xie, *Nanoscale*, 2013, **5**, 5241-5246.

5   J. Wang, N. Yang, H. Tang, Z. Dong, Q. Jin, M. Yang, D. Kisailus, H. Zhao, Z. Tang and D. Wang, *Angew. Chem.*, 2013, **125**, 6545-6548.

6   Y. Wang, F. Yan, S. W. Liu, A. Y. S. Tan, H. Song, X. W. Sun and H. Y. Yang, *J. Mater. Chem. A*, 2013, **1**, 5212-5216.

7   S.-W. Bian and L. Zhu, *RSC Adv.*, 2013, **3**, 4212-4215.

8   Q. Hao, M. Li, S. Jia, X. Zhao and C. Xu, *RSC Adv.*, 2013, **3**, 7850-7854.

9   M. Y. Son, Y. J. Hong and Y. C. Kang, *Chem. Commun.*, 2013, **49**, 5678-5680.

10   Y. Wang, H. J. Zhang, J. Wei, C. C. Wong, J. Lin and A. Borgna, *Energy Environ. Sci.*, 2011, **4**, 1845-1854.

11   S. Xiong, J. S. Chen, X. W. Lou and H. C. Zeng, *Adv. Funct. Mater.*, 2012, **22**, 861-871.

12   S. Yang, G. Cui, S. Pang, Q. Cao, U. Kolb, X. Feng, J. Maier and K. Müllen, *ChemSusChem*, 2010, **3**, 236-239.

13   S. Yang, X. Feng, S. Ivanovici and K. Müllen, *Angew. Chem.*, 2010 **122**, 8586-8589.

14   X. Wang, X.-L. Wu, Y.-G. Guo, Y. Zhong, X. Cao, Y. Ma and J. Yao, *Adv. Funct. Mater.*, 2010, **20**, 1680-1686.

15   S.-L. Li and Q. Xu, *Energy Environ. Sci.*, 2013, **6**, 1656-1683.

16   M. Sindoro, N. Yanai, A.-Y. Jee and S. Granick, *Acc. Chem. Res.*, 2013, **47**, 459-469.

17   M. Hu, J. Reboul, S. Furukawa, N. L. Torad, Q. Ji, P. Srinivasu, K. Ariga, S. Kitagawa and Y. Yamauchi, *J. Am. Chem. Soc.*, 2012, **134**, 2864-2867.

18   X. Xu, R. Cao, S. Jeong and J. Cho, *Nano Lett.*, 2012, **12**, 4988-4991.

19   W. Chaikittisilp, K. Ariga and Y. Yamauchi, *J. Mater. Chem. A*, 2013, **1**, 14-19.

20   L. Zhang, H. B. Wu, S. Madhavi, H. H. Hng and X. W. Lou, *J. Am. Chem. Soc.*, 2012, **134**, 17388-17391.

21   R. Wu, X. Qian, F. Yu, H. Liu, K. Zhou, J. Wei and Y. Huang, *J. Mater. Chem. A*, 2013, **1**, 11126-11129.

22   W. Chaikittisilp, M. Hu, H. Wang, H.-S. Huang, T. Fujita, K. C. W. Wu, L.-C. Chen, Y. Yamauchi and K. Ariga, *Chem. Commun.*, 2012, **48**, 7259-7261.

23   W. Cho, Y. H. Lee, H. J. Lee and M. Oh, *Adv. Mater.*, 2011, **23**, 1720-1723.

24   L. Hu, Y. Huang, F. Zhang and Q. Chen, *Nanoscale*, 2013, **5**, 4186-4190.

25   L. Hu and Q. Chen, *Nanoscale*, 2014, **6**, 1236-1257.

26   N. L. Torad, M. Hu, Y. Kamachi, K. Takai, M. Imura, M. Naito and Y. Yamauchi, *Chem. Commun.*, 2013, **49**, 2521-2523.

27   Z. Jiang, Z. Li, Z. Qin, H. Sun, X. Jiao and D. Chen, *Nanoscale*, 2013, **5**, 11770-11775.

28   J.-U. Park, H. J. Lee, W. Cho, C. Jo and M. Oh, *Adv. Mater.*, 2011, **23**, 3161-3164.

29   J. Li, J. Wang, X. Liang, Z. Zhang, H. Liu, Y. Qian and S. Xiong, *ACS Appl. Mater. Interfaces*, 2013, **6**, 24-30.

30   L. Zhou, D. Zhao and X. W. Lou, *Adv. Mater.*, 2012, **24**, 745-748.

31   R. Wang, C. Xu, J. Sun, Y. Liu, L. Gao and C. Lin, *Nanoscale*, 2013, **5**, 6960-6967.

32   F. Zhan, B. Geng and Y. Guo, *Chem. Eur. J.*, 2009, **15**, 6169-6174.

33   J. Maier, *Nat. Mater.*, 2005, **4**, 805-815.

34   S. Laruelle, S. Grugeon, P. Poizot, M. Dolle, L. Dupont and J.-M. Tarascon, *J. Electrochem. Soc.*, 2002, **149**, A627-A634.

35   Yan-Yan Hu, Z. Liu, K. W. Nam, O. J. Borkiewicz, J. Cheng, X. Hua, M. T. Dunstan, X. Yu, K. M. Wiaderek, L.-S. Du, K. W. Chapman, P. J. Chupas, X. Q. Yang and C. P. Grey, *Nat. Mater.*, 2013, **12**, 1130-1136.

36   K. M. Shaju, F. Jiao, A. Debart and P. G. Bruce, *Phys. Chem. Chem. Phys.*, 2007, **9**, 1837-1842.

37   N. Liu, H. Wu, M. T. McDowell, Y. Yao, C. Wang and Y. Cui, *Nano Lett.*, 2012,

12, 3315-3321.
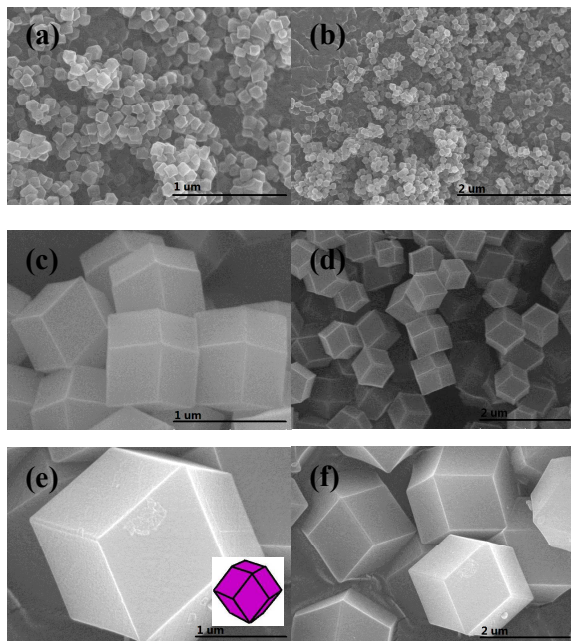
Fig. 1 SEM images of (a, b) small-sized, (c, d) middle-sized, and (e, f) large-sized ZIF-67 rhombic dodecahedrons. The inset in Fig. 1e shows the simulated dodecahedral structure of ZIF-67.
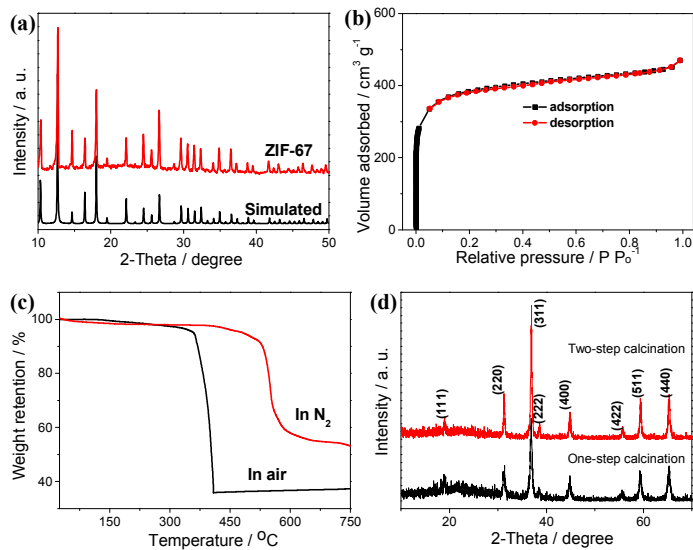
Fig. 2 (a) XRD pattern of ZIF-67. (b) N_2 adsorption/desorption isotherm of ZIF-67. (c) TG curves of ZIF-67 under air and nitrogen atmosphere. (d) XRD patterns of two Co_3O_4 samples obtained through one-step and two-step calcination of ZIF-67.
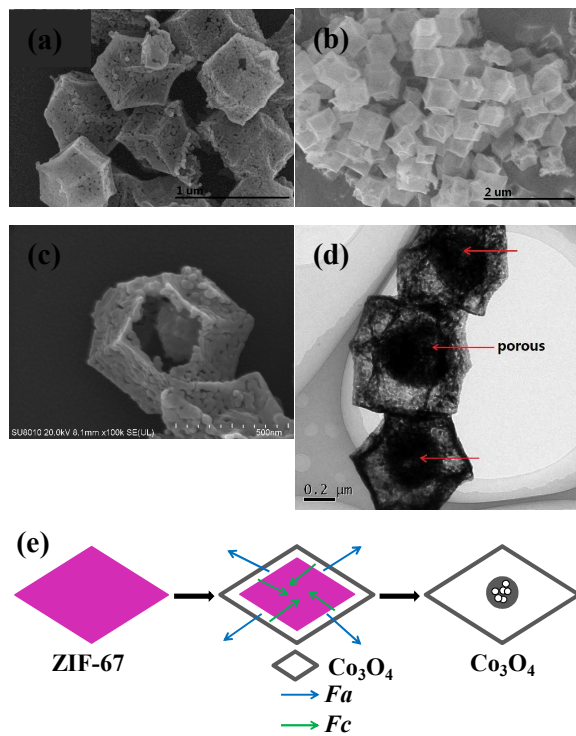
Fig. 3 (a-c) SEM and (d) TEM images of Co_3O_4 obtained through one-step calcination

of ZIF-67. (e) Schematic illustration of the formation of ball-in-dodecahedron Co_3O_4.
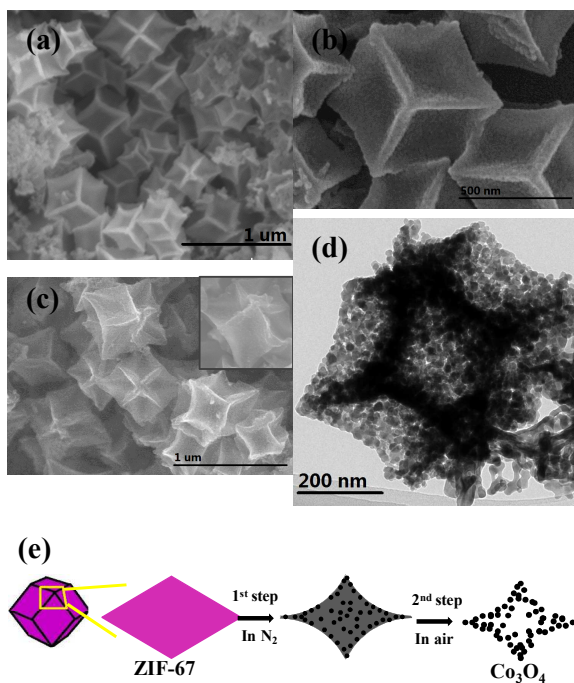
Fig. 4 (a, b) SEM images of Co_3O_4 obtained through two-step calcination of ZIF-67.

(c) SEM image of the intermediate product after the first-step calcination of ZIF-67

under N_2 atmosphere. (d) TEM image of Co_3O_4. (e) Schematic illustration of the

formation of Co_3O_4 dodecahedrons with concave surfaces.
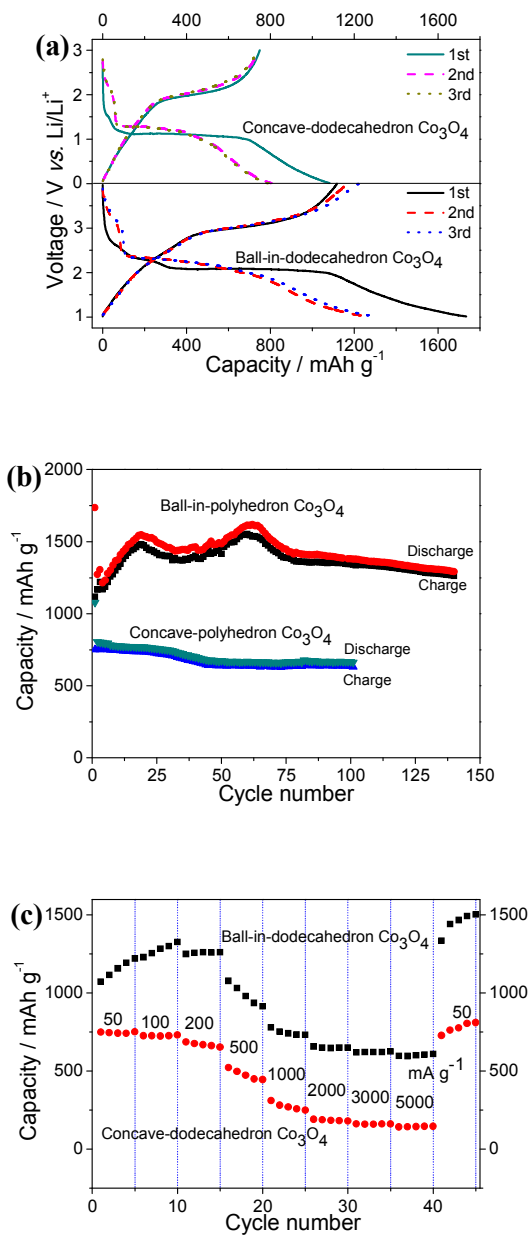
Fig. 5 (a) The initial three discharge/charge curves, (b) long-term cycling performance,

and (c) rate behaviors of ball-in-dodecahedron and concave-dodecahedron Co_3O_4.

For Table of Content use
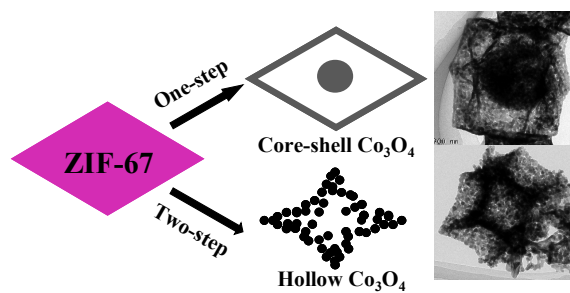
Co_3O_4 hollow dodecahedrons with controllable interiors are prepared through direct pyrolysis of ZIF-67 and exhibit high performance for Li-ion storage.